Characterizing mouse platelet heterogeneity across diverse disease models using spectral flow cytometry and high-dimensional analysis

Received: 11 September 2025 | Revised: 22 November 2025 | Accepted: 24 December 2025

https://doi.org/10.1016/j.rpth.2026.103371

METHODOLOGICAL ARTICLE

Characterizing mouse platelet heterogeneity across diverse disease models using spectral flow cytometry and high-dimensional analysis

Deepa Gautam[1,2] | Emily M. Clarke[1] | Rebecca L. Zon[1,2,3] | Margaret R. Smith-Oliver[1,2] | Avinash Kumar[5] | Megan E. Sullivan[1] | Panagiotis Karagiannis[2,3] | Harvey G. Roweth[1,2,4] | Elisabeth M. Battinelli[1,2]

[1]Division of Hematology, Brigham and Women's Hospital, Boston, Massachusetts, USA

[2]Harvard Medical School, Boston, Massachusetts, USA

[3]Department of Medical Oncology, Dana-Farber Cancer Institute, Boston, Massachusetts, USA

[4]School of Biological Sciences, University of Reading, Reading, UK

[5]Innotone.ai, Bengaluru, India

Correspondence
Elisabeth M. Battinelli, Brigham and Women's Hospital, Mass General Brigham, Harvard Medical School, Boston, MA 02115, USA.
Email: embattinelli@bwh.harvard.edu

Handling Editor: Dr Carsten Depperman

Abstract

Background: Routine platelet assessment based on count and mean platelet volume overlooks heterogeneity of platelet subpopulations that influence disease outcomes. Different platelet subtypes are associated with diverse pathological conditions, highlighting the need to define and characterize them. Human studies face limitations due to interindividual variability and challenges in acquiring matched controls. Moreover, the small and anucleate nature of platelets constrain conventional single-cell analysis approaches. These gaps highlight the need for a mouse-specific flow cytometry panel to enable detailed investigation of platelet heterogeneity in preclinical models.

Objectives: To develop and validate a mouse-specific spectral flow cytometry panel integrated with a high-dimensional analysis pipeline for comprehensive characterization of platelet subpopulations and activation states under physiological and pathological conditions.

Methods: A 12-marker spectral panel was optimized and integrated with the PlateletProfiler pipeline for multidimensional clustering and receptor expression profiling. The workflow was applied to conditions known to alter platelet dynamics, including agonist-induced activation and three mouse models of disease: lipopolysaccharide-induced inflammation, *Jak2V617F* driven myeloproliferative neoplasms, and breast cancer.

Results: Four major platelet subpopulations-resting, primed, aggregatory, and procoagulant-were identified, representing a continuum of activation. Lipopolysaccharide exposure increased primed and aggregatory subsets, *Jak2V617F* mice showed aggregatory and procoagulant fractions, and tumor-bearing mice exhibited increased procoagulant platelets. Across models, platelets displayed upregulation of activation and procoagulant markers. All disease models displayed elevated thiazole orange-positive reticulated platelets.

Harvey Roweth and Elisabeth Battinelli contributed equally as co-senior authors.

Conclusions: This integrated and scalable workflow provides a robust platform for investigating disease-associated changes in platelet heterogeneity. The PlateletProfiler pipeline is compatible with both mouse and human datasets, supporting broad experimental and translational applications.

KEYWORDS
breast cancer, flow cytometry, inflammation, lipopolysaccharide, platelet

Essentials

- Routine blood tests miss diverse platelet types that can affect disease risk.
- We designed a mouse antibody panel and PlateletProfiler pipeline to map platelets.
- We identified different platelet subtypes and showed how they change in disease.
- We can also study differences in surface receptors between these different platelet subtypes.

1 | INTRODUCTION

Once regarded as uniform cellular fragments primarily involved in clot formation and hemostasis, platelets are now recognized as functionally diverse cells that contribute to immune regulation [1–3], inflammation [4–6], and tissue remodeling [7–9]. Along with this, the concept of platelet heterogeneity has been under investigation for decades [10–12], with growing experimental evidence supporting the existence of functionally specialized subpopulations [13–15].

Under normal physiological conditions, most circulating platelets remain in a resting state, characterized by a discoid morphology and lacking surface expression of activation markers. This resting phenotype enables platelets to circulate freely without initiating clot formation [16]. However, upon encountering external stimuli, including biochemical signals or environmental stress, platelets become activated. The strength and nature of these stimuli determine the expression of surface receptors, leading to diverse functional phenotypes. Among these, the aggregatory and procoagulant phenotypes, which are central to thrombus formation, have been the most extensively studied [17,18]. Strongly activated platelets are cleared from circulation, and the bone marrow responds by releasing reticulated platelets (RPs), which are immature fraction that indicate platelet turnover [19]. In several pathological conditions, altered subpopulations of circulating platelets have been reported to impact disease severity and clinical outcomes [20–27]. These observations underline the importance of precise phenotyping of circulating platelets to better understand their role in disease. Addressing this could pave the way for targeted therapies aimed not just at platelets broadly, but at the subpopulations most involved in disease progression.

To facilitate detailed analysis of platelet subpopulations, we developed a mouse-specific spectral flow cytometry panel comprising 12 carefully selected markers. These markers target key surface receptors involved in platelet activation, adhesion, immune regulation, and procoagulant functions. The panel includes CD62P (P-selectin) [28], CD107a (LAMP-1) [29], GPVI [30], CD36 [31], CD29 (β1 integrin) [32], CD42a [33], CD32 (FcγRII) [34], PD-L1 (CD274) [35], and CD154 (CD40L) [36]. The panel also includes annexin V for assessing phosphatidylserine (PS) exposure, fibrinogen binding for detecting integrin activation, and thiazole orange (TO) staining to indicate residual RNA content. This panel is integrated with an analytical platform called PlateletProfiler, which allows the classification of platelet subpopulations based on activation markers and PS exposure. It quantifies the proportion of each subtype present and maps the expression profiles of various receptors across these subpopulations. Moreover, it allows for the comparison of receptor expression under different physiological and pathological conditions, providing a comprehensive overview of platelet heterogeneity and activation dynamics.

To explore the utility of this panel and PlateletProfiler, 3 well-established mouse models were studied. These included lipopolysaccharide (LPS)-induced systemic inflammation [37], *Jak2V617F* driven myeloproliferation [38], and breast tumor growth [39,40], each known to influence platelet phenotype and function. Overall, this platform enables detailed profiling of platelet subtypes and activation in health and disease.

2 | METHODS

2.1 | Panel development

Detailed information on all antibodies used in this study are provided in the Table and Supplementary Table 1. To investigate platelet heterogeneity, we designed and optimized antibody staining panels using a 4-laser Cytek Aurora spectral flow cytometer (405, 488, 561, and 640 nm; Cytek Biosciences). Fluorochrome selection was guided by spectral uniqueness, assessed using Cytek's similarity index

TABLE Functional characterization of markers used in the mouse platelet panel.

Markers	Biological Roles
Annexin V	Binds phosphatidylserine in apoptotic cells; depicts procoagulant platelets; essential for accelerating thrombin generation and stabilizing fibrin formation
CD62P (P-selectin)	Reflects the degranulation of α-granule during early activation. Plays a role in leukocyte recruitment to sites of injury and inflammation
CD107a (LAMP-1)	Indicator of platelet activation and degranulation of lysosome; immune response modulation; platelet adhesion
CD31	Involved in platelet aggregation, endothelial cell adhesion, and transendothelial migration
CD42a	Part of the GPIb-IX-V complex; initiates platelet adhesion to vascular injuries
CD32 (FcγRII)	Allows platelets to recognize immune complexes and modulate interactions with leukocytes via Fc receptor-mediated signaling, contributing to inflammatory responses
GPVI	Major collagen receptor involved in platelet activation, adhesion, and aggregation at sites of vascular injury
CD154 (CD40L)	An immune costimulatory molecule expressed on activated platelets, is known to influence endothelial activation, antigen-presenting cell maturation, and B-cell responses, establishing a link between platelet activity and adaptive immunity
CD36	A scavenger receptor, contributes to platelet adhesion and amplifies signaling responses under proinflammatory and prothrombotic conditions, particularly through interactions with oxidized lipids and thrombospondin
Fibrinogen	Binds to the integrin α_{IIb} β_3, reflecting the platelet's ability to aggregateand to form stable platelet-platelet interactions
CD274 (PD-L1)	Modulates the immune response by inhibiting T-cell activation and proliferation
CD29 (β1 integrin)	Facilitates platelet adhesion to extracellular matrix proteins such as fibronectin and collagen, supporting thrombus formation and stabilization under flow
Thiazole orange	Stains nucleic acids

The table lists the selected markers used in the panel along with their biological roles. Markers were chosen to capture diverse platelet functions including activation, adhesion, aggregation, immune modulation, and procoagulant activity, enabling comprehensive phenotypic profiling of platelet subpopulations under various conditions.

CD, cluster of differentiation; CD40L, CD40 ligand; CD62P, CD62 antigen-like family member P; GP, glycoprotein; LAMP-1, lysosome-associated membrane protein 1; PD-L1, programmed death-ligand 1.

(Supplementary Table 2), which ranges from 0 (completely nonoverlapping spectra) to 1 (identical spectra). Panel compatibility was further evaluated using the complexity index, which estimates spectral interference and predicts the impact of autofluorescence and spillover on unmixing accuracy.

2.2 | Antibody titration

Precise antibody titration is essential for achieving optimal performance of the spectral flow cytometry panel. Antibodies were titrated for optimal staining that provided clear separation between positive and negative populations, as previously described [41]. To quantify the effectiveness of each antibody concentration, we calculated the Separation Index (*SI*) as follows: *SI* = (Median positive – Median negative)/((84th percentile of Median negative – Median negative))/0.995, as described previously [41]. A higher *SI* indicates enhanced spectral separation, facilitating more accurate phenotyping. For activation markers, the maximum *SI* (SI_{max}) was selected to ensure discrimination of activated from nonactivated platelet populations. For constitutive markers, a threshold of *SI* >1 was deemed adequate to differentiate specific binding from background fluorescence effectively.

2.3 | Mouse platelet preparation

Whole blood was collected from 10- to 14-week-old male or female mice through intracardiac puncture using syringes containing 3.2% w/v sodium citrate. Blood was then diluted 1:1 with Tyrode's buffer (20 mM HEPES, 138 mM NaCl, 2.9 mM KCl, 1 mM $MgCl_2$, 0.36 mM NaH_2PO_4, 5 mM glucose, pH 7.4). To separate platelet-rich plasma from red and white blood cells, diluted blood was centrifuged at 200 × *g* for 10 minutes at room temperature (RT). For platelet isolation, prostaglandin E1 (1 μmol/L; Sigma-Aldrich; P5515) was added to platelet-rich plasma, which was then centrifuged at 400 × *g* for 10 minutes at RT. The resulting platelet pellet was resuspended in Tyrode's buffer and the platelet concentration normalized to 2 × 10^8/mL using a Cytek Aurora flow cytometer. Isolated platelets were utilized within 3 hours of blood collection to ensure their functionality.

2.4 | Multi-antibody staining of platelets

Antibodies were diluted in Tyrode's buffer supplemented with 2.5 mM calcium chloride. For each experimental setup, 10 μL platelets (2 × 10^8 cells/mL) were incubated with 50 μL antibody cocktail for 10

min at RT in the dark to allow antibody binding to surface antigens on platelets. In experiments requiring platelet activation, samples were treated with collagen-related peptide (CRP-A) (Pplus Medical; CRP-A0.5-WIN03) at 1 μg/mL or with a combination of CRP-A and 0.1 U/mL thrombin (Sigma-Aldrich; T4648-1KU), followed by incubation for 10 minutes at RT. Platelet nucleic acids were stained with thiazole orange (TO) (Sigma-Aldrich; 390062) at 200 ng/mL for 10 min, followed by fixation with 2% (w/v) paraformaldehyde in phosphate-buffered saline (PBS) (Thermo Fisher Scientific; J19943-K2). Fixed platelets were resuspended in 250 μL Hank's Balanced Salt Solution and transferred to 5-mL Falcon round-bottom polystyrene test tubes. The Cytek Aurora spectral cytometer was employed to acquire 50,000 events per sample at a low flow rate.

2.5 | Single-stained reference control

Single-stained controls were prepared using platelet samples to establish spectral reference signatures. Each antibody was diluted in Tyrode's buffer with 2.5 mM calcium chloride and combined with 10 μL platelets in a 1.5-mL Eppendorf tube. The mixture was incubated in the dark at RT for 10 minutes to allow antibody binding. For antibodies detecting activation-dependent markers, CRP-A was added at a final concentration of 1 μg/mL, and samples were incubated for an additional 15 minutes. Samples were then fixed with 2% w/v paraformaldehyde and resuspended in Hank's Balanced Salt Solution for acquisition, as described in the previous section.

2.6 | Evaluation of unmixing quality and marker performance

Spectral unmixing was carried out using Cytek Aurora SpectroFlo software (version 2.2). To minimize background interference and enhance signal clarity, autofluorescence extraction was applied across the panel. Platelets were gated, and fluorescence peaks from each fluorophore were individually assessed to ensure clear separation of signal from background and accurate identification of each marker. The spectral signature of each marker was cross-checked against expected emission profiles, and all gating positions were visually reviewed across samples to maintain consistency and data integrity.

2.7 | TO gating

TO fluorescence was measured in the B3 channel (Alexa Fluor 532), where it exhibits peak emission (554 nm). A fluorescence intensity histogram was generated, and the top 5% to 7% of the brightest events were gated to define the TO-positive platelet population, following previously established methods [42].

2.8 | High-dimensional data analysis and characterization of platelet subpopulations

Spectral flow cytometry data were analyzed using a custom-built Python platform, PlateletProfiler, developed with the Streamlit framework. FCS files were first processed using FlowJo v10, where initial gating and quality control were performed. Platelets were identified based on forward and side scatter properties and further gated on CD42a-positive events to ensure platelet specificity and minimize background noise. For each mouse, 10,000 CD42a-positive platelet events were exported as CSV files. These files, containing marker expression measurements, were then uploaded for further preprocessing, including optional subsampling to manage large datasets and improve computational efficiency. Data subsampling was performed in 2 stages. First, 10,000 rows were read from each input file, each corresponding to a different experimental condition. These rows were then aggregated across all input files. From the combined dataset, a fixed number of samples was randomly selected for downstream analysis. To normalize feature distributions, compress dynamic range, and preserve zero or negative values, the subsampled data were then transformed using the hyperbolic arcsine (asinh) function with a user-defined cofactor. This transformation enhanced the interpretability and performance of subsequent clustering analyses. Following transformation, unsupervised clustering was performed using the KMeans algorithm (scikit-learn), grouping data points based on multivariate marker expression profiles. Dimensionality reduction was achieved using Uniform Manifold Approximation and Projection (UMAP). An integrated annotation module, built using Fabric.js, enabled interactive editing and labeling of plots directly within the application. All Analyses were conducted utilizing standard Python-3.11.11 libraries including Pandas, NumPy, scikit-learn, umap-learn, Matplotlib, Seaborn, and Plotly. The PlateletProfiler analysis pipeline is an in-house tool and is not publicly available as open-source software.

2.9 | Experimental mouse models

All animal experiments were performed in accordance with relevant guidelines and regulations and were approved by the Brigham and Women's Hospital Institutional Animal Care and Use Committee (protocol No. 2019N000011). C57BL/6 wildtype mice (RRID: IMSR_JAX:000664) were purchased from The Jackson Laboratories. To create an inflammatory model, each mouse was administered 0.5 mg/kg LPS or a sterile PBS vehicle control intraperitoneally as previously described [43]. A mouse model carrying the *Jak2V617F* mutation, commonly used to study myeloproliferative neoplasms (MPN), was developed by Ann Mullaly, as previously described [44]. For establishing a breast cancer tumor model, 2.5×10^5 EO771 cells were prepared in PBS and injected into the fourth left mammary fat pad of 7- to 8-week-old C57BL/6 females. Tumor growth became

palpable approximately 7 to 10 days postinjection, after which tumor volume was measured every other day. Mice were euthanized after EO771 injection when tumor growth reached the predefined humane endpoint. Inclusion or exclusion criteria were not applicable for animal studies. A total of 5 mice per group were used for the CRP-A/thrombin, *Jak2V617F*, and tumor-bearing mouse experiments, while 4 mice were used for the LPS experiment.

2.10 | Statistical analysis

All statistical analyses and graphical representations were performed using GraphPad Prism (version 10.1.1), while UMAP plots were generated within the PlateletProfiler application. Information regarding biological replicates, sources of variability, and *P* values are provided within the figures and their corresponding legends. For comparisons between 2 independent groups, unpaired two-tailed *t*-tests were applied to normally distributed data, while the nonparametric Mann–Whitney U-test was used for nonnormally distributed datasets. In cases in which fold changes were analyzed, paired one-sample *t*-tests or Wilcoxon signed-rank tests were conducted, depending on data distribution. Throughout all analyses, statistical significance was determined using a threshold of $P \leq .05$.

3 | RESULTS

3.1 | Optimization of antibody concentrations for spectral flow cytometry panel design

To enable accurate and reproducible profiling of platelet phenotypes using spectral flow cytometry, we performed antibody titration for both constitutive and activation-dependent antigens (Figure 1). The chosen concentrations reflect conditions that provided maximal or sufficient *SI*, balancing signal resolution with minimal background as described in the Methods. Particular attention was given to antibodies with reported activating effects on platelets, such as CD36 [45] and GPVI [46]. These antibodies were carefully titrated in the presence of anti-CD62P antibody to ascertain concentrations that yield optimal staining while precluding inadvertent platelet activation. As shown in Supplementary Figure S1, no significant activation was observed, supporting their use at the selected concentrations.

3.2 | Visualization and classification of platelet subpopulations

To examine how platelet subpopulation dynamics change with increasing levels of activation, we analyzed 3 conditions that represent a gradient of stimulation. These included an unstimulated baseline, mild stimulation with CRP-A (1 μg/mL), and strong stimulation using a combination of CRP-A and thrombin (0.1 U/mL). Spectral flow cytometry followed by high-dimensional analysis was performed on pooled platelet samples from all 3 conditions. Based on the expression of activation markers and PS exposure, 4 platelet subpopulations were identified and categorized as resting, primed, aggregatory, and procoagulant (Figure 2A, B).

Key differences in CD62P and GPVI expression, fibrinogen binding, and PS exposure formed the basis for distinguishing the platelet subpopulations (Supplementary Figure S2A, B). Resting platelets lacked activation markers, reflecting a quiescent state. Primed platelets exhibited moderate levels of CD62P and fibrinogen binding and retained GPVI expression, indicating an early activation state without PS exposure. Aggregatory platelets displayed high levels of CD62P, fibrinogen binding, and GPVI, consistent with a strong activation profile but no PS exposure. Procoagulant platelets were annexin V-positive and included 2 subsets, 1 expressing high levels of CD62P, fibrinogen, and GPVI (procoagulant-1) and another lacking both activation markers and GPVI (procoagulant-2). Detailed analysis of receptor expression showed that the identified platelet subpopulations display varied surface marker profiles, indicating differences in their activation states (Supplementary Figure S2A, C).

To examine how platelet subpopulations are distributed across baseline and activated states, we segregated the pooled data points (Figure 2C). The relative proportions of each subpopulation in these conditions are shown in the stacked bar graph (Figure 2D). Under unstimulated conditions (Figure 2Ci), most platelets remained in a resting state (68.1%), with a notable proportion classified as primed (23.1%). Only a small fraction of platelets displayed aggregatory (8.7%) or procoagulant (0.1%) characteristics, reflecting a baseline, low-activation phenotype. Upon CRP-A stimulation (Figure 2Cii), there was a marked shift toward the aggregatory phenotype, with 78.6% of platelets classified as aggregatory. The resting (4.7%) and primed (14.4%) populations were reduced accordingly. A small proportion (2.3%) transitioned into the procoagulant state, consistent with previous reports that a low dose of CRP-A alone induces aggregation-dominant activation with limited procoagulant conversion [47]. Costimulation with CRP-A and thrombin (Figure 2Ciii) resulted in a pronounced redistribution toward the procoagulant phenotype, which constituted 55.3% of all platelets. A substantial fraction also remained in the aggregatory state (37.2%), whereas only a small minority persisted as resting (4.7%) or primed (2.8%). This observation aligns with prior findings showing that simultaneous activation of thrombin and collagen receptors strongly promotes procoagulant platelet formation [48].

3.3 | Agonist-dependent modulation of surface receptor expression

It is well established that surface receptor expression on platelets changes dynamically upon agonist stimulation [49]. To investigate this further, we performed high-dimensional analysis to study the expression of both activation and constitutive markers under unstimulated and stimulated conditions. The expression of surface receptors across

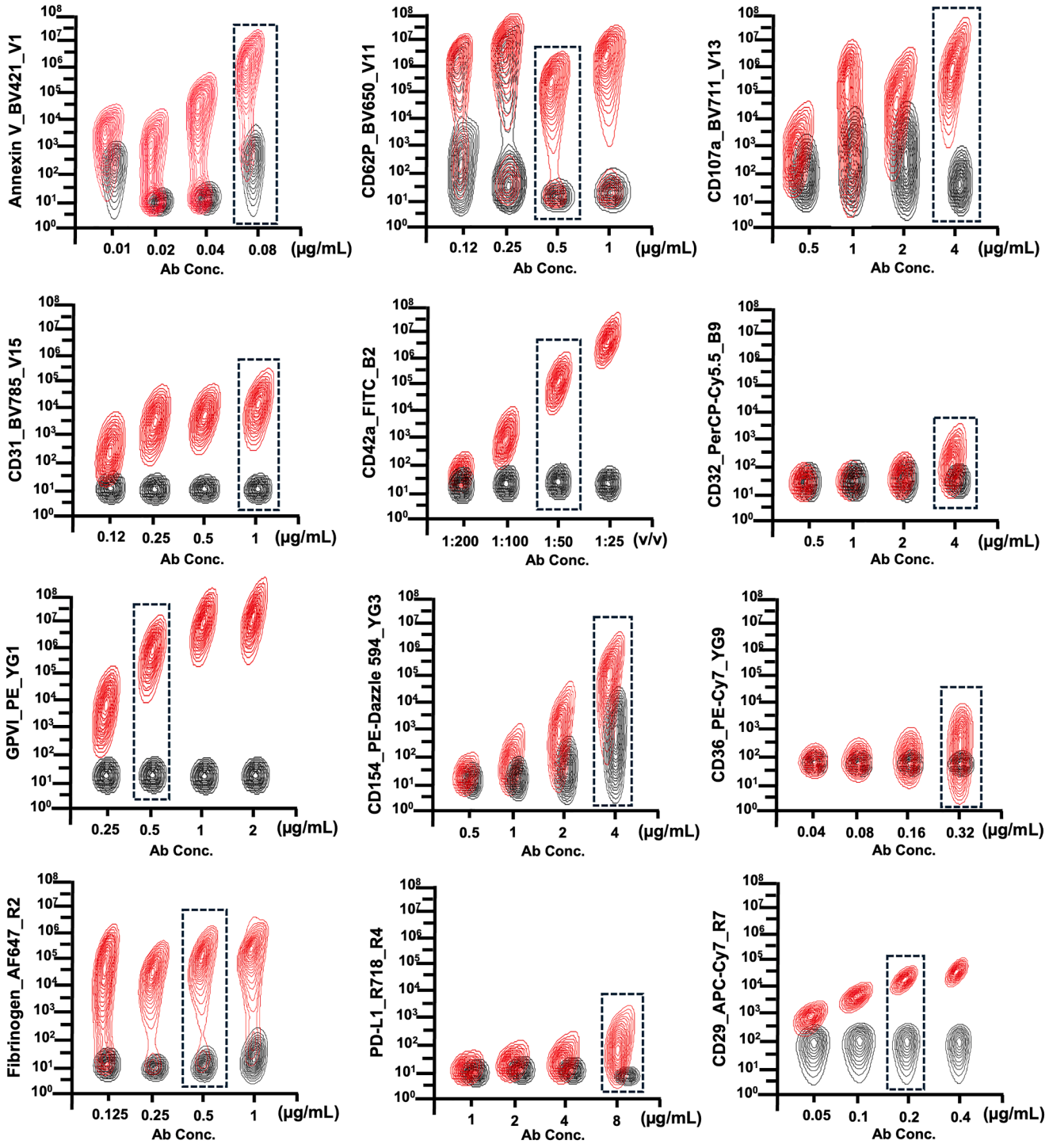

FIGURE 1 Antibody titration and optimization of surface marker concentrations. Contour plots display the fluorescence intensity of platelets stained with increasing concentrations of individual antibodies targeting platelet surface markers. For constitutive markers (CD31, CD42a, GPVI, CD36, and CD29), red contours represent stained platelets, and black contours represent unstained controls. For activation-dependent markers (annexin V, CD62P [P-selectin], CD107a, CD32, CD154, fibrinogen, and PD-L1 [programmed death-like ligand 1]), red contours represent collagen-related peptide (1 µg/mL) stimulated platelets, while black contours represent unstimulated, antibody-stained platelets. Optimal antibody concentrations were determined based on separation index, with the selected concentrations indicated by dashed black boxes. Ab Conc., antibody concentration.

the 3 treatment conditions is shown in the heatmap (Figure 2E) and the bar graph (Figure 2F). In unstimulated platelets, activation markers were expressed at minimal levels. CRP-A stimulation resulted in a significant increase in fibrinogen and annexin V binding, alongside elevated expression of activation markers such as CD62P, PD-L1, CD107a, CD154, and the constitutive marker CD36. These markers

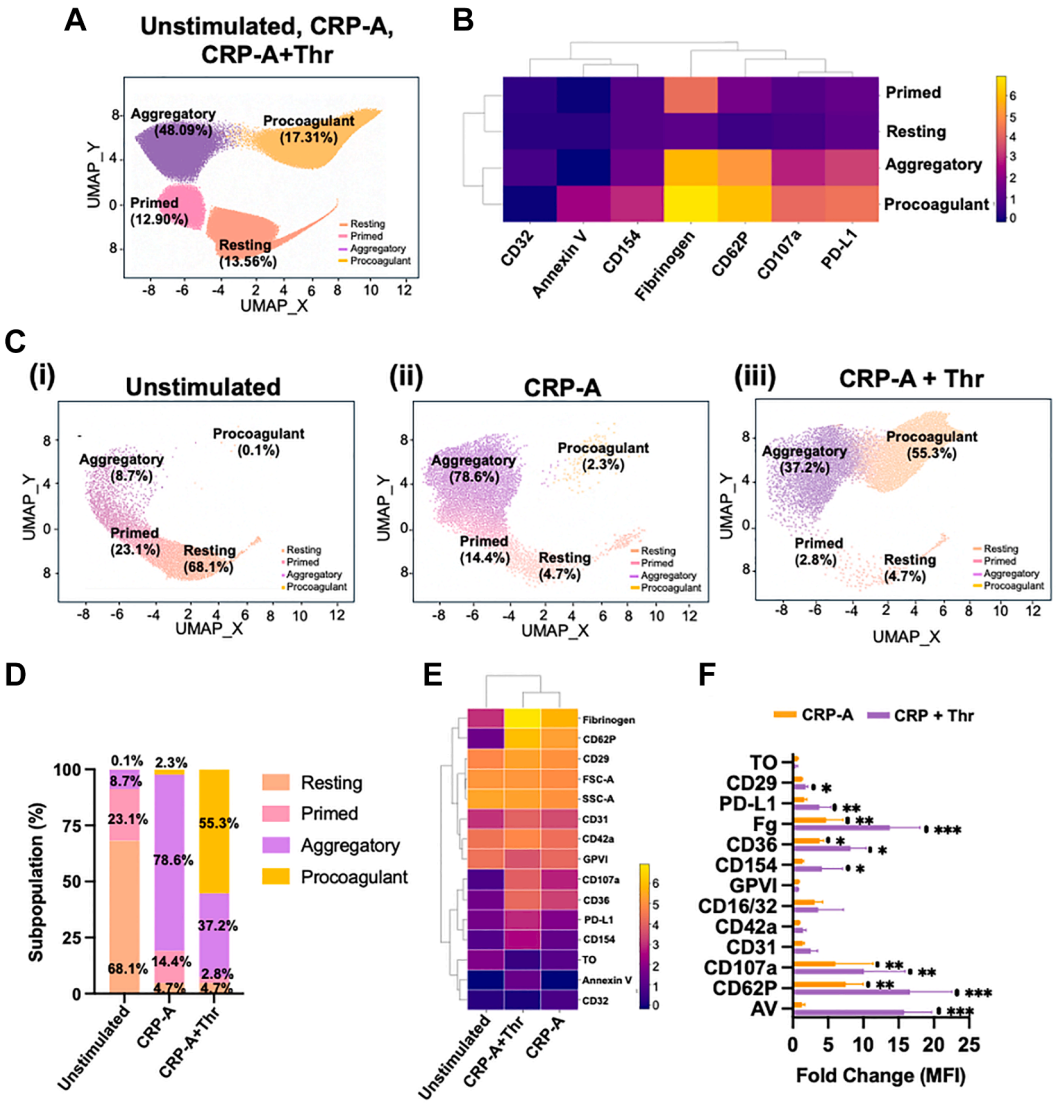

FIGURE 2 High-dimensional analysis depicts dynamic redistribution of platelet subpopulations under different stimulation conditions. (A) UMAP showing the combined clustering of platelets pooled from all 3 experimental conditions (unstimulated, CRP-A [1 μg/mL] and CRP-A + Thr [0.1 U/mL]) based on surface marker expression. Clusters were classified into resting, primed, aggregatory, and procoagulant subpopulations according to activation marker profiles. (B) Heatmap displaying the expression levels (mean fluorescence intensity) of selected activation markers across the 4 platelet subtypes, highlighting the phenotypic differences among clusters. (C) UMAP of platelets under 3 conditions: (i) unstimulated, (ii) stimulated with CRP-A, and (iii) costimulated with CRP-A + Thr, showing redistribution among subpopulations. (D) Stacked bar plot showing the percentage of each platelet subpopulation across the 3 conditions. (E) Heatmap illustrating changes in marker expression across treatment conditions. (F) Bar graph representing fold changes in surface receptor expression (MFI) for CRP-A and CRP-A+ Thr-treated platelets relative to the unstimulated control (baseline, fold change = 1). Markers with statistically significant changes are denoted. Statistical analysis was performed using paired one-sample *t*-tests and Wilcoxon signed-rank tests (n = 5 mice per condition). Error bars represent mean ± SD. $^{*}P \leq .05$, $^{**}P \leq .01$, $^{***}P \leq .001$. AV, annexin V; CRP, collagen-related peptide; Fg, fibrinogen; GPVI, glycoprotein VI; MFI, mean fluorescence intensity; PD-L1, programmed death-like ligand 1; Thr, thrombin; TO, thiazole orange; UMAP, Uniform Manifold Approximation and Projection.

were further upregulated upon dual stimulation with CRP-A and thrombin. Notably, markers such as CD154 and PD-L1 showed marked increases only under costimulation conditions. Upon dual stimulation, platelets showed reduced TO staining (Figure 2E), indicating lower RNA content and suggesting a shift toward terminal activation. Dual stimulation resulted in a decrease in GPVI expression, as observed in the heat map (Figure 2E).

3.4 | Application of PlateletProfiler across diverse mouse models of disease

We applied the spectral flow cytometry panel to three disease models including LPS-induced inflammation, *Jak2V617F*-driven myeloproliferation, and breast cancer. Using PlateletProfiler, we analyzed platelet subpopulation distribution and surface receptor

expression to explore changes in platelet phenotype and activation in these pathological conditions.

3.4.1 | LPS-induced inflammation drives a shift toward aggregatory platelet phenotypes

Six hours after LPS injection, platelet counts in these mice were significantly reduced compared with those receiving PBS (Supplementary Figure S3A). In LPS-injected mice, the majority of circulating platelets were either in a primed (41.9%) or aggregatory (40%) state, whereas only a small proportion remained resting (18.1%). In contrast, PBS-injected mice predominantly exhibited a resting subset (84.2%), with smaller fractions in primed (10.5%) and aggregatory (5.3%) states (Figure 3A, B). Analysis of platelet surface markers revealed that LPS exposure led to a modest increase in P-selectin levels but significantly enhanced fibrinogen binding (Figure 4Ai, ii). In addition, expression levels of PD-L1, CD36, and CD154 was significantly elevated after LPS treatment (Figure 4Ai, ii).

3.4.2 | *Jak2V617F* mutation promotes aggregatory and procoagulant platelet phenotypes

Circulating platelets from *Jak2V617F* mutant mice exhibited a notable shift in subpopulation distribution compared to Vav/Cre controls (Figure 3C, D). While control mice showed a predominance of resting platelets (81.1%), *Jak2V617F* mice displayed a marked reduction in this population (45.7%) and a substantial increase in aggregatory (34.0%) and procoagulant-1 and -2 (2.1%) subsets, indicating a shift toward a more activated platelet phenotype. The primed population remained similar between groups (16.9% vs 18.2%). To further characterize this altered profile, we analyzed surface marker expression and found increased fibrinogen binding and increased expression of CD31, CD29, CD42a, PD-L1, CD154, CD62P, CD107a, and CD36 on platelets from *Jak2V617F* mice (Figure 4Bi, ii).

3.4.3 | Breast tumors induce a procoagulant platelet phenotype

Mice injected with EO771 cells developed tumors averaging ~1000 mm^3 by day 30 (Supplementary Figure S3B). Analysis of circulating platelet subpopulations revealed dynamic alterations in breast tumor-bearing mice compared with controls (Figure 3E, F). In control mice, most platelets were in a resting state (75.6%), followed by primed platelets (23.2%), with aggregatory (1.1%) and small fractions of the procoagulant (0.1%) subset. In breast tumor-bearing mice, the overall distribution shifted modestly, with resting platelets comprising 72.5% of the population and an increase in procoagulant-1 and -2 platelets to 6.0%, indicating tumor-associated formation of procoagulant platelets. The proportions of primed (19.6%) and aggregatory platelets (1.8%) remained unchanged. To further characterize these alterations, we assessed the expression of key constitutive and activation-associated markers. Platelets from breast tumor-bearing mice showed reduced CD31 expression and elevated CD42a levels compared with controls, with both changes reaching statistical significance (Figure 4Ci, ii).

3.5 | Increased reticulated platelets and variable receptor expression in 3 experimental models representing inflammatory, myeloproliferative, and tumor conditions

TO-high (reticulated) platelets represent a younger, more reactive subpopulation that is frequently elevated in conditions associated with increased platelet turnover, such as inflammation, myeloproliferative disorders, and cancer. To characterize newly formed RPs, we analyzed TO staining in platelets and surface receptor expression in the top 5%-7% of platelets exhibiting the highest TO fluorescence across all 3 disease models. TO fluorescence intensity was significantly elevated in each model compared with its respective control (Figure 5A–C). Concordantly, the proportion of TO-high platelets was greater in LPS-treated, *Jak2V617F*, and tumor-bearing mice relative to their respective controls (Figure 5D–F). In LPS-injected mice, RPs showed increased fibrinogen binding and elevated expression of CD62P, PD-L1, CD36, CD42a, CD107a, CD154, and CD29 (Figure 5G). In the *Jak2V617F* model, RPs similarly showed enhanced fibrinogen binding along with higher expression of CD62P, CD36, CD107a and CD29. Markedly, this model also demonstrated a significant reduction in GPVI expression (Figure 5H). In the breast tumor-bearing model, RPs showed a substantial increase in CD42a expression and a significant decrease in CD31 expression, whereas the expression of other markers remained unchanged (Figure 5I).

4 | DISCUSSION

The spectral flow cytometry panel and PlateletProfiler platform developed in this study offer a resolute, high-dimensional solution for characterizing mouse platelet heterogeneity with single-cell resolution, providing insight into the pathophysiology of platelets in unique disease states. Unlike prior approaches, this system enables simultaneous assessment of activation states and surface receptor dynamics across large datasets, facilitating the identification of different platelet subpopulations.

Our analysis identified different platelet subpopulations comprising resting, primed, aggregatory, and procoagulant that reflect a continuum of activation states (Figure 2B and Supplementary Figure S2). Among these, the primed population represents an intermediate functional state characterized by partial fibrinogen binding and limited degranulation, suggesting early responsiveness to mild physiological triggers. They reflect the temporal differences in receptor mobilization, where fibrinogen binding occurs rapidly following mild stimulation, whereas P-selectin exposure requires more sustained activation [50]. Previous

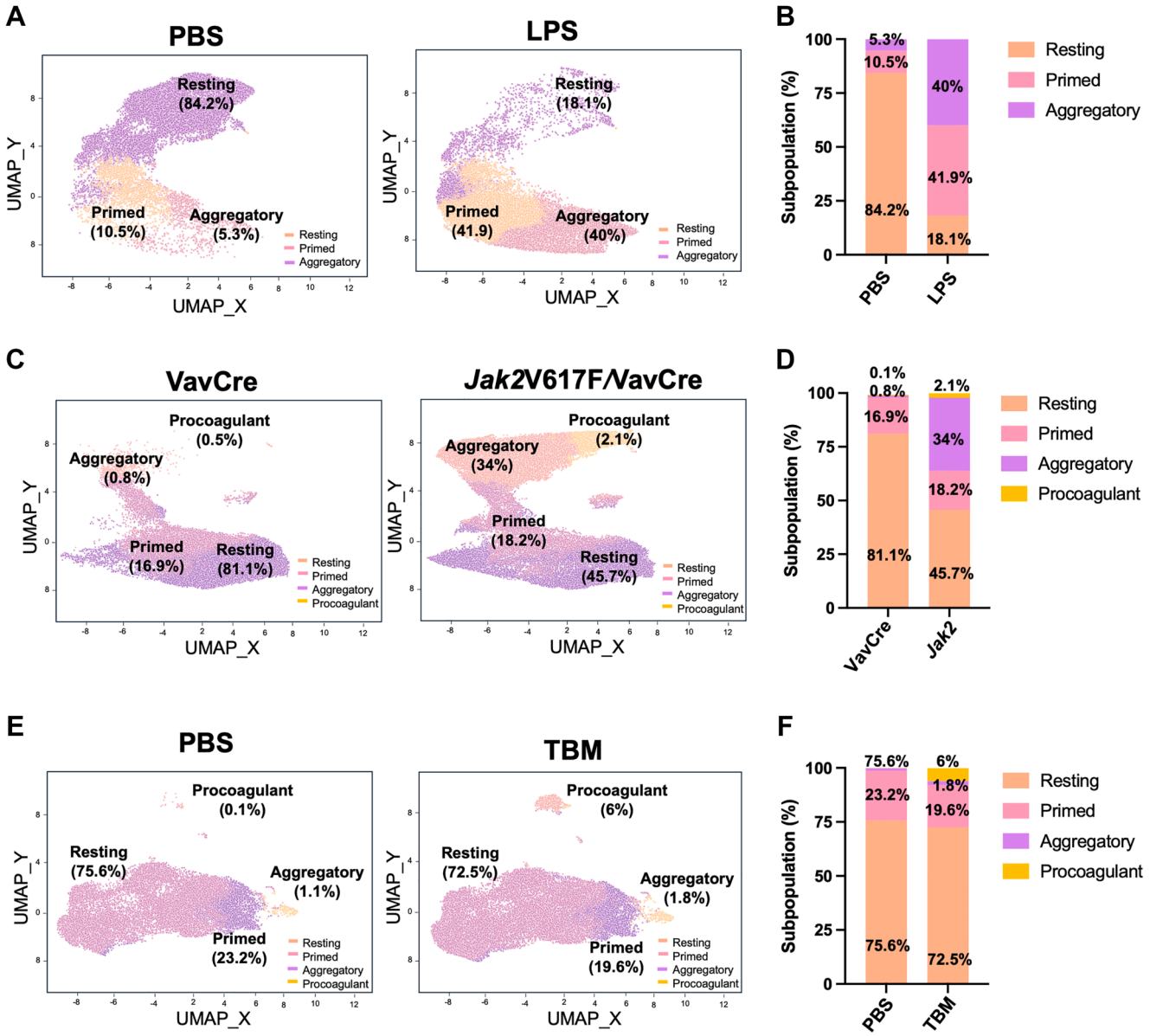

FIGURE 3 Uniform Manifold Approximation and Projection (UMAP)-based analysis of platelet subpopulations across disease models. (A) UMAP showing the distribution of platelet subpopulations in phosphate-buffered saline (PBS)- vs lipopolysaccharide (LPS)-treated mice, with the percentage of each subpopulation indicated (n = 4 per group). (B) Stacked bar graph comparing the proportion of platelet subpopulations between PBS- and LPS-treated groups. (C) UMAP showing platelet subpopulation distribution in VavCre and *Jak2V617F*/VavCre mice (n = 5 per group). (D) Stacked bar graph illustrating the proportions of platelet subpopulations in VavCre vs *Jak2V617F*/VavCre mice. (E) UMAP of platelet subpopulations in PBS-treated vs tumor-bearing mice (TBM). (F) Stacked bar graph showing the percentage distribution of platelet subpopulations in PBS- and TBM- groups.

studies have shown that inhibiting P-selectin can disrupt established platelet aggregates, illustrating its role in stabilizing platelet-platelet interactions during later stages of activation [50]. Our data also expand the phenotypic definition of procoagulant platelets, a population known to play significant roles in the pathophysiology of prothrombotic diseases [27,51–53]. Although previous studies have identified procoagulant platelets based on annexin V, P-selectin, and fibrinogen expression [14], we demonstrated additional upregulation of PD-L1, CD107a, CD36, CD154, and CD42a within this subpopulation (procoagulant-1), markers not previously linked to the procoagulant phenotype (Figure 2B and Supplementary Figure S2). This coexpression pattern suggests that procoagulant platelets may contribute not only to coagulation but also to immune modulation and inflammatory signaling, particularly under pathological conditions. We also identified a smaller subset of annexin V-positive platelets lacking all other activation markers (procoagulant-2) (Supplementary Figure S2), corresponding to apoptotic-like platelets [54]. Notably, this annexin V-positive subpopulation exhibited markedly reduced GPVI expression, a finding not previously described at this resolution. This phenotype likely reflects strong platelet activation, as GPVI is known to undergo shedding or

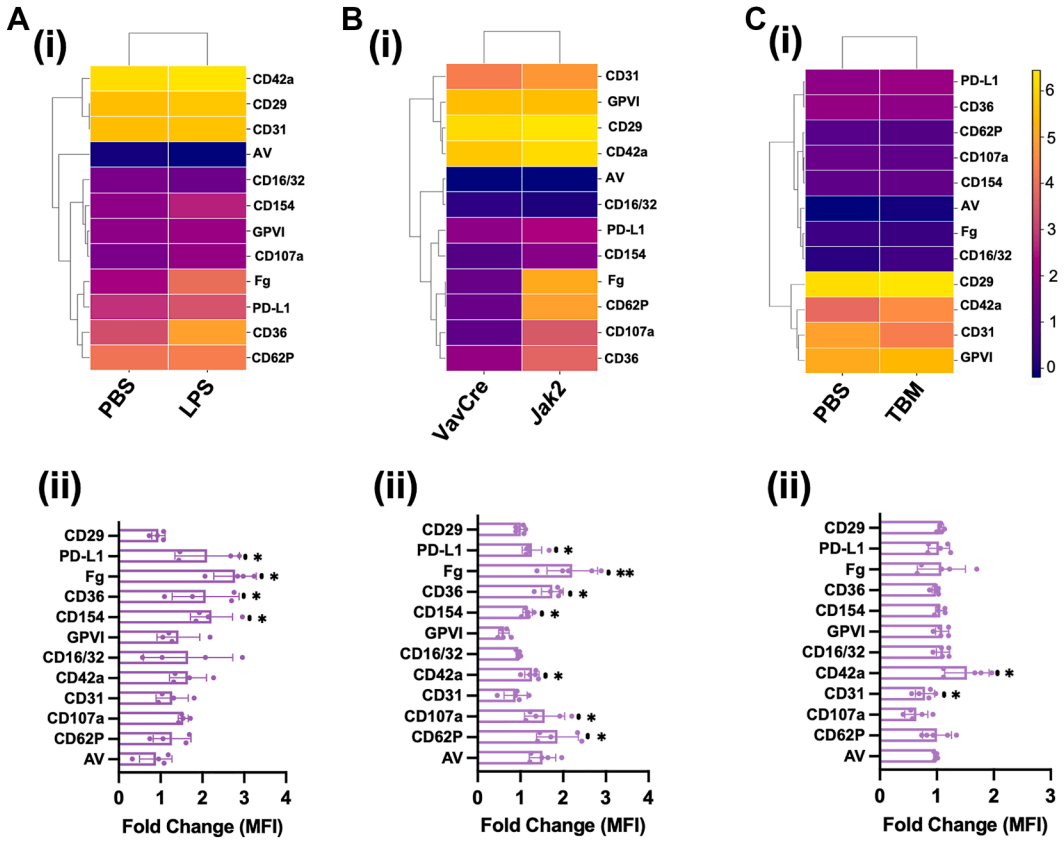

FIGURE 4 Surface marker expression profiling across disease models. (A) (i) Heatmap showing fold changes in surface receptor expression (mean fluorescence intensity, MFI) in platelets from lipopolysaccharide (LPS)-treated vs phosphate-buffered saline (PBS)-treated control mice (n = 4 per group). (ii) Corresponding bar graph quantifying fold changes in individual markers relative to PBS control. (B) (i) Heatmap showing fold changes in platelet surface marker expression between *Jak2V617F*/VavCre and VavCre mice (n = 5 per group). (ii) Bar graph depicting fold changes in specific markers relative to VavCre control. (C) (i) Heatmap showing surface marker expression changes in platelets from tumor-bearing mice (TBM) compared with PBS-treated controls (n = 5 per group). (ii) Bar graph showing fold change in marker expression relative to PBS control. Fold change values are relative to the control group, which was set as the baseline (fold change = 1). Statistical significance was determined using paired one-sample t-tests and Wilcoxon signed-rank tests. Error bars represent mean ± SD. $^{*}P \leq .05$, $^{**}P \leq .01$. AV, annexin V; Fg, fibrinogen; GPVI, glycoprotein VI; PD-L1, programmed death-like ligand 1.

internalization under such conditions [55] (Supplementary Figure S2A, B). Together, these findings demonstrate the capability of our panel and PlateletProfiler to map platelet activation trajectories and heterogeneity by capturing both established and novel subpopulations defined by marker expression profiles.

To explore how these subpopulations behave in pathology, we next examined platelet profiles across 3 different mouse models including LPS-induced inflammation, *Jak2V617F*-driven myeloproliferation, and breast cancer. In parallel, we examined RPs, a population of newly formed and RNA-rich platelets that are often increased in diseases [38,56,57] and may show altered surface receptor expression.

In the LPS-induced model of inflammation we observed a reduction in circulating platelet counts (Supplementary Figure S3), consistent with platelet consumption or sequestration during inflammatory responses [37]. This decline in platelet numbers is attributed to LPS-induced platelet activation, which typically leads to platelet consumption and removal from circulation [43,58]. This was accompanied by a pronounced shift toward primed and aggregatory subpopulations (Figure 3A, B), reflecting elevated platelet activation. These changes align with previous reports in humans and mice linking LPS-induced platelet activation to enhanced granule secretion and integrin activation through downstream effectors [59,60]. Although LPS exposure led to only a modest increase in P-selectin expression, it substantially enhanced fibrinogen binding on platelets (Figure 4Ai, ii), suggesting that LPS preferentially primes integrin activation pathways. This is consistent with an earlier study showing similar platelet responses after LPS treatment [43]. In addition to classical activation markers such as CD154 and CD107a, which are associated with platelet degranulation and inflammatory signaling [61], we noticed a notable upregulation of PD-L1 (Figure 4Ai, ii). Given the established role of PD-L1 in immune checkpoint regulation and suppression of T cell responses [35,62–65], its presence on platelets suggests a potential immunomodulatory role during inflammation.

To assess how chronic hematopoietic dysregulation influences platelet heterogeneity, we examined platelet profile in *Jak2V617F* mutant mice, a model of MPNs. These mice exhibited a marked shift in subpopulation distribution with a notable expansion of aggregatory and procoagulant subsets (Figure 3C, D), suggesting an

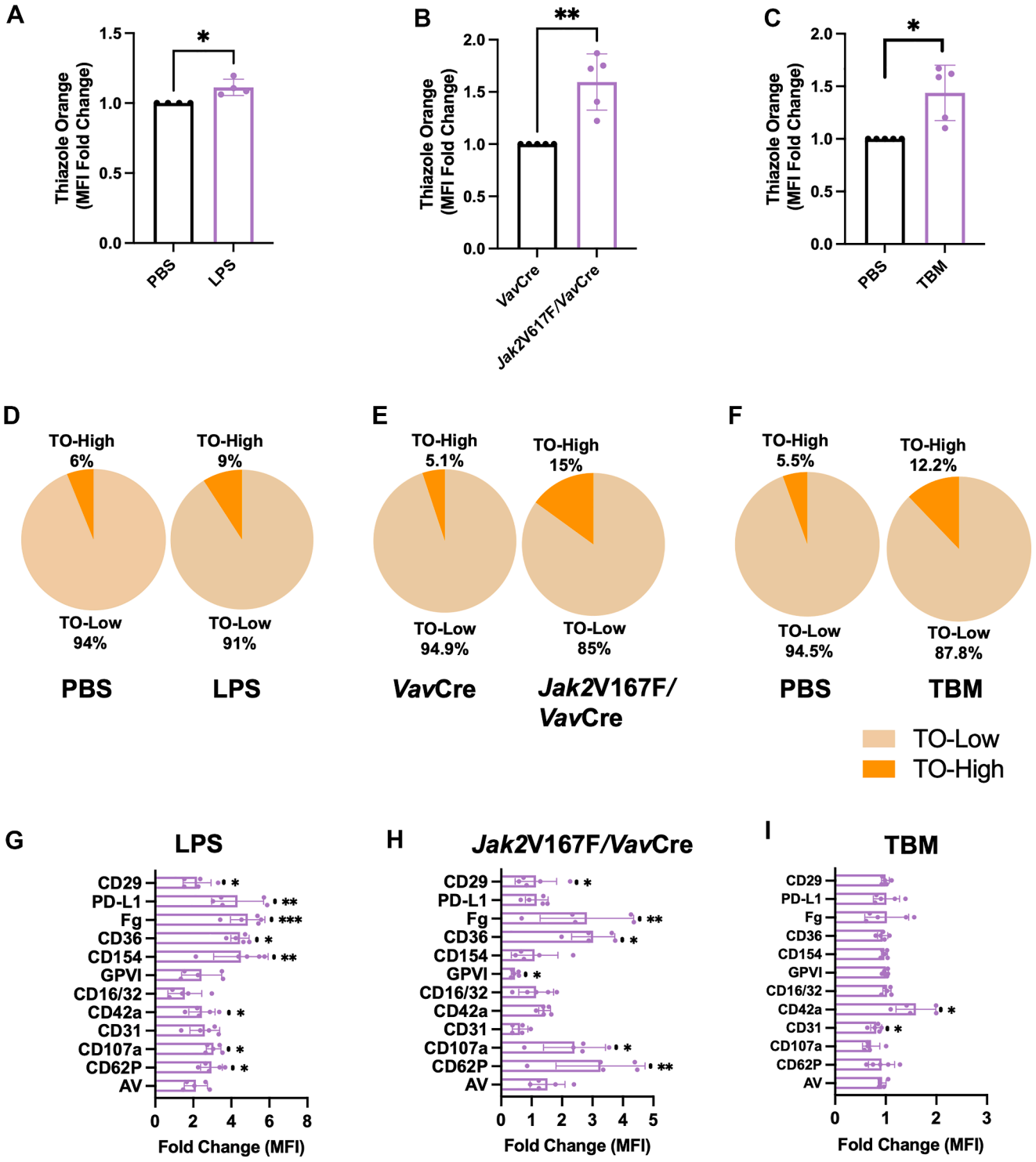

FIGURE 5 Increased RNA content and surface receptor expression in TO-high platelets across inflammatory, myeloproliferative, and tumor models. Thiazole orange (TO) mean fluorescence intensity (MFI) fold change showing increased RNA content in platelets from (A) phosphate-buffered saline (PBS)- and lipopolysaccharide (LPS)-treated mice, (B) VavCre and *Jak2V617F*/VavCre mice, and (C) PBS-treated and tumor-bearing mice (TBM). Pie charts depicting the proportion of immature (TO-high) vs mature (TO-low) platelets from (D) PBS- and LPS-treated mice, (E) VavCre and *Jak2V617F*/VavCre mice, and (F) PBS-treated mice and TBM. Fold change in surface receptor expression on TO-high platelets in (D) PBS- and LPS-treated mice, (E) VavCre and *Jak2V617F*/VavCre mice, and (F) PBS-treated mice and TBM. For LPS, n = 4 mice per group; *Jak2V617F*/VavCre, n = 5 per group; TBM, n = 5 mice per group. In all cases, fold change values are shown relative to control group (baseline = 1). Data represent mean ± SD. Statistical analysis was performed using paired one-sample t-tests and Wilcoxon signed-rank tests. Error bars represent mean ± SD. $^{*}P < .05$, $^{**}P < .01$, $^{***}P < .001$.

increased baseline activation state. This profile mirrors the prothrombotic phenotype reported in patients with MPNs carrying the *JAK2V617F* mutation and in the corresponding mouse model, linking the mutation to increased thrombotic risk, enhanced platelet activation, and elevated procoagulant activity [38,66–68]. Elevated fibrinogen binding and P-selectin expression on platelets from *Jak2V617F*-mutant mice (Figure 4Bi, ii) suggest enhanced platelet reactivity, consistent with observations in patients with MPNs [66,68]. The upregulation of CD36 and CD154 (Figure 4Bi, ii) further supports the presence of activated platelets that may contribute to the prothrombotic environment associated with *JAK2* mutations [66,69].

To further explore how tumor burden influences platelet phenotypes, we analyzed platelets from breast tumor-bearing mice. These mice exhibited a slight increase in procoagulant platelets (Figure 3E, F), potentially contributing to both the hypercoagulable environment and immune evasion commonly associated with malignancy [52,70]. Cancer-associated thrombosis is a major cause of morbidity and mortality in cancer patients and arises from tumor-driven inflammation, tissue factor expression, and platelet activation that together enhance thrombin generation. The increase in procoagulant platelets observed here provides a mechanistic link to this process, as these platelets expose PS and promote fibrin formation [71,72]. In addition, platelets from tumor-bearing mice exhibited reduced CD31 expression (Figure 4Ci, ii). This observation is supported by previous studies showing that activated platelets can shed CD31 from their surface [73]. Similar shedding of CD31 has also been reported in other activated cells, including T cells [74].

All 3 disease models showed an increased proportion of RPs (Figure 5A–F), indicating enhanced platelet turnover. This is consistent with previous studies suggesting increased thrombopoiesis in response to inflammatory or pathological stress [57,75]. This immature platelet fraction exhibited elevated expression of activation markers (Figure 5G–I), suggesting an activated state that may contribute to thromboinflammatory complications.

Our spectral flow cytometry panel and PlateletProfiler platform enable characterization of platelet subpopulation distributions across physiological and pathological conditions. This approach facilitates the study of surface receptor expression, protein binding, and activation profiles within different subsets, revealing how platelet heterogeneity shifts in disease. Such insights may support future efforts to link specific subpopulation patterns to clinical outcomes and identify liquid biomarkers. The panel is flexible, allowing users to incorporate markers of interest, and the PlateletProfiler is compatible with both mouse and human platelets, making it broadly applicable for investigating platelet biology across species.

ACKNOWLEDGMENTS

We thank A. Mullally, B. Rolles, and A. Hillerbrand for providing the *Jak2* mice.

FUNDING

This work was supported by the Cancer Research Institute through award number CRI4828. R. L. Zon is supported by the Mark Foundation for Cancer Research Physician-Scientist of the Damon Runyon Cancer Research Foundation (PST-44-24) and the Edward P. Evans Foundation Young Investigator Award.

AUTHOR CONTRIBUTIONS

D.G., E.M.B., and H.G.R. proposed the research. D.G. designed and performed experiments, analyzed data, and wrote the manuscript, with experimental assistance from E.M.C., R.L.Z., M.R.S.-O., and P.K. A.K. contributed to the development of the PlateletProfiler platform. E.M.B. provided critical resources. H.G.R. and E.M.B. offered valuable input on the research design and manuscript. H.G.R. and R.L.Z. reviewed the manuscript. E.M.C. and M.E.S. assisted with editing the manuscript. M.E.S. helped perform the experiments during the revision. All authors read and approved the final version of the article.

RELATIONSHIP DISCLOSURE

There are no conflicts of interest.

DECLARATION OF GENERATIVE AI AND AI-ASSISTED TECHNOLOGIES IN THE WRITING PROCESS

During the preparation of this work, the authors used ChatGPT-5 to check grammar and improve readability. After using this tool, the authors reviewed and edited the content as needed and take full responsibility for the content of the publication.

ORCID

Deepa Gautam https://orcid.org/0000-0003-2437-6136

REFERENCES

[1] Tyagi T, Jain K, Yarovinsky TO, Chiorazzi M, Du J, Castro C, et al. Platelet-derived TLT-1 promotes tumor progression by suppressing $CD8^+$ T cells. *J Exp Med*. 2023;220:e20212218. https://doi.org/10.1084/jem.20212218

[2] Chen X, Xu Y, Chen Q, Zhang H, Zeng Y, Geng Y, et al. The phosphatase PTEN links platelets with immune regulatory functions of mouse T follicular helper cells. *Nat Commun*. 2022;13:2762. https://doi.org/10.1038/s41467-022-30444-y

[3] Lutz MS, Klimovich B, Maurer S, Heitmann JS, Märklin M, Zekri L, et al. Platelets subvert antitumor efficacy of T cell-recruiting bispecific antibodies. *J Immunother Cancer*. 2022;10:e003655. https://doi.org/10.1136/jitc-2021-003655

[4] Rolfes V, Ribeiro LS, Hawwari I, Böttcher L, Rosero N, Maasewerd S, et al. Platelets Fuel the Inflammasome Activation of Innate Immune Cells. *Cell Rep*. 2020;31:107615. https://doi.org/10.1016/j.celrep.2020.107615

[5] Thornton P, McColl BW, Greenhalgh A, Denes A, Allan SM, Rothwell NJ. Platelet interleukin-1α drives cerebrovascular inflammation. *Blood*. 2010;115:3632–9.

[6] Lindemann S, Tolley ND, Dixon DA, McIntyre TM, Prescott SM, Zimmerman GA, et al. Activated platelets mediate inflammatory signaling by regulated interleukin 1beta synthesis. *J Cell Biol*. 2001;154:485–90.

[7] Stellos K, Kopf S, Paul A, Marquardt JU, Gawaz M, Huard J, et al. Platelets in regeneration. *Semin Thromb Hemost*. 2010;36:175–84.
[8] Murata S, Ohkohchi N, Matsuo R, Ikeda O, Myronovych A, Hoshi R. Platelets promote liver regeneration in early period after hepatectomy in mice. *World J Surg*. 2007;31:808–16.
[9] Crowley ST, Dempsey EC, Horwitz KB, Horwitz LD. Platelet-induced vascular smooth muscle cell proliferation is modulated by the growth amplification factors serotonin and adenosine diphosphate. *Circulation*. 1994;90:1908–18.
[10] Penington DG, Streatfield K, Roxburgh AE. Megakaryocytes and the heterogeneity of circulating platelets. *Br J Haematol*. 1976;34:639–53.
[11] Rand ML, Packham MA, Mustard JF. Survival of density subpopulations of rabbit platelets: use of ^{51}Cr-or ^{111}In-labeled platelets to measure survival of least dense and most dense platelets concurrently. *Blood*. 1983;61:362–7.
[12] Karpatkin S. Heterogeneity of human platelets. I. Metabolic and kinetic evidence suggestive of young and old platelets. *J Clin Invest*. 1969;48:1073–82.
[13] Vadgama A, Boot J, Dark N, Allan HE, Mein CA, Armstrong PC, et al. Multiparameter phenotyping of platelets and characterization of the effects of agonists using machine learning. *Res Pract Thromb Haemost*. 2024;8:102523. https://doi.org/10.1016/j.rpth.2024.102523
[14] Hindle MS, Spurgeon BEJ, Cheah LT, Webb BA, Naseem KM. Multidimensional flow cytometry reveals novel platelet subpopulations in response to prostacyclin. *J Thromb Haemost*. 2021;19:1800–12.
[15] Johnson L, Lei P, Waters L, Padula MP, Marks DC. Identification of platelet subpopulations in cryopreserved platelet components using multi-colour imaging flow cytometry. *Sci Rep*. 2023;13:1221. https://doi.org/10.1038/s41598-023-28352-2
[16] Thomas SG. The structure of resting and activated platelets. In: Michelson AD, ed. *Platelets*. 4th ed. San Diego, CA: Academic Press (Elsevier); 2019:47–77.
[17] Heemskerk JWM, Mattheij NJA, Cosemans JMEM. Platelet-based coagulation: different populations, different functions. *J Thromb Haemost*. 2013;11:2–16.
[18] Agbani EO, Poole AW. Procoagulant platelets: generation, function, and therapeutic targeting in thrombosis. *Blood*. 2017;130:2171–9.
[19] Ma R, Xie R, Yu C, Si Y, Wu X, Zhao L, et al. Phosphatidylserine-mediated platelet clearance by endothelium decreases platelet aggregates and procoagulant activity in sepsis. *Sci Rep*. 2017;7:4978. https://doi.org/10.1038/s41598-017-04773-8
[20] Qiu X, Nair MG, Jaroszewski L, Godzik A. Deciphering abnormal platelet subpopulations in COVID-19, sepsis and systemic lupus erythematosus through machine learning and single-cell transcriptomics. *Int J Mol Sci*. 2024;25:5941. https://doi.org/10.3390/ijms25115941
[21] Lee CSM, Estabrooks KL, Lai K, Dey A, Cheng J, Whittaker S, et al. Procoagulant platelet subpopulation as a novel predictive biomarker of poor outcomes in essential thrombocythemia. *Blood*. 2021;138(Suppl 1):3622.
[22] Prodan CI, Stoner JA, Cowan LD, Dale GL. Higher coated-platelet levels are associated with stroke recurrence following nonlacunar brain infarction. *J Cereb Blood Flow Metab*. 2013;33:287–92.
[23] Kirkpatrick AC, Tafur AJ, Vincent AS, Dale GL, Prodan CI. Coated-platelets improve prediction of stroke and transient ischemic attack in asymptomatic internal carotid artery stenosis. *Stroke*. 2014;45:2995–3001.
[24] Prodan CI, Joseph PM, Vincent AS, Dale GL. Coated-platelets in ischemic stroke: differences between lacunar and cortical stroke. *J Thromb Haemost*. 2008;6:609–14.
[25] Zanetto A, Toffanin S, Campello E, Radu CM, Gavasso S, Burra P, et al. Reticulated platelets are increased and hyper-activated in patients with cirrhosis, especially those with poor outcome. *Dig Liver Dis*. 2024;56:1327–34.
[26] Butt AJ, Zaidi U, Munawar Ali R, Zafar S, Ali MS, Shamsi T. Reticulated Platelet count as a diagnostic tool in immune thrombocytopenia (ITP). *Cureus*. 2023;15:e41346. https://doi.org/10.7759/cureus.41346
[27] Kaiser R, Dewender R, Mulkers M, Stermann J, Rossaro D, Di Fina L, et al. Procoagulant platelet activation promotes venous thrombosis. *Blood*. 2024;144:2546–53.
[28] McEver RP, Martin MN. A monoclonal antibody to a membrane glycoprotein binds only to activated platelets. *J Biol Chem*. 1984;259:9799–804.
[29] Malik A, Sayed AA, Han P, Tan MMH, Watt E, Constantinescu-Bercu A, et al. The role of CD8$^+$ T-cell clones in immune thrombocytopenia. *Blood*. 2023;141:2417–29.
[30] Massberg S, Gawaz M, Grüner S, Schulte V, Konrad I, Zohlnhöfer D, et al. A crucial role of glycoprotein VI for platelet recruitment to the injured arterial wall in vivo. *J Exp Med*. 2003;197:41–9.
[31] Chen Y, Zhang J, Cui W, Silverstein RL. CD36, a signaling receptor and fatty acid transporter that regulates immune cell metabolism and fate. *J Exp Med*. 2022;219:e20211314. https://doi.org/10.1084/jem.20211314
[32] Varga-Szabo D, Pleines I, Nieswandt B. Cell adhesion mechanisms in platelets. *Arterioscler Thromb Vasc Biol*. 2008;28:403–12.
[33] Li R, Emsley J. The organizing principle of the platelet glycoprotein Ib-IX-V complex. *J Thromb Haemost*. 2013;11:605–14.
[34] Tomiyama Y, Kunicki TJ, Zipf TF, Ford SB, Aster RH. Response of human platelets to activating monoclonal antibodies: importance of FcγRII (CD32) phenotype and level of expression. *Blood*. 1992;80:2261–8.
[35] Rolfes V, Idel C, Pries R, Plötze-Martin K, Habermann J, Gemoll T, et al. PD-L1 is expressed on human platelets and is affected by immune checkpoint therapy. *Oncotarget*. 2018;9:27460–70.
[36] Cognasse F, Duchez AC, Audoux E, Ebermeyer T, Arthaud CA, Prier A, et al. Platelets as key factors in inflammation: focus on CD40L/CD40. *Front Immunol*. 2022;13:825892. https://doi.org/10.3389/fimmu.2022.825892
[37] Zhao L, Ohtaki Y, Yamaguchi K, Matsushita M, Fujita T, Yokochi T, et al. LPS-induced platelet response and rapid shock in mice: contribution of O-antigen region of LPS and involvement of the lectin pathway of the complement system. *Blood*. 2002;100:3233–9.
[38] Liu W, Pircher J, Schuermans A, Ul Ain Q, Zhang Z, Honigberg MC, et al. *Jak2^{V617F}* clonal hematopoiesis promotes arterial thrombosis via platelet activation and cross talk. *Blood*. 2024;143:1539–50.
[39] Tang Y, Qian C, Zhou Y, Yu C, Song M, Zhang T, et al. Activated platelets facilitate hematogenous metastasis of breast cancer by modulating the PDGFR-β/COX-2 axis. *iScience*. 2023;26:107704. https://doi.org/10.1016/j.isci.2023.107704
[40] Kassassir H, Karolczak K, Siewiera KM, Wojkowska DW, Braun M, Watala CW. Time-dependent interactions of blood platelets and cancer cells, accompanied by extramedullary hematopoiesis, lead to increased platelet activation and reactivity in a mouse orthotopic model of breast cancer - implications for pulmonary and liver metastasis. *Aging (Albany NY)*. 2020;12:5091–120.
[41] Spurgeon BEJ, Frelinger AL. OMIP-097: High-parameter phenotyping of human platelets by spectral flow cytometry. *Cytometry A*. 2023;103:935–40.
[42] Kienast J, Schmitz G. Flow cytometric analysis of thiazole orange uptake by platelets: a diagnostic aid in the evaluation of thrombocytopenic disorders. *Blood*. 1990;75:116–21.
[43] Andonegui G, Kerfoot SM, McNagny K, Ebbert KVJ, Patel KD, Kubes P. Platelets express functional Toll-like receptor-4. *Blood*. 2005;106:2417–23.

[44] Mullally A, Lane SW, Ball B, Megerdichian C, Okabe R, Al-Shahrour F, et al. Physiological *Jak2V617F* expression causes a lethal myeloproliferative neoplasm with differential effects on hematopoietic stem and progenitor cells. *Cancer Cell*. 2010;17:584–96.
[45] Ockenhouse CF, Magowan C, Chulay JD. Activation of monocytes and platelets by monoclonal antibodies or malaria-infected erythrocytes binding to the CD36 surface receptor in vitro. *J Clin Invest*. 1989;84:468–75.
[46] Boylan B, Berndt MC, Kahn ML, Newman PJ. Activation-independent, antibody-mediated removal of GPVI from circulating human platelets: development of a novel NOD/SCID mouse model to evaluate the in vivo effectiveness of anti-human platelet agents. *Blood*. 2006;108:908–14.
[47] Ollivier V, Syvannarath V, Gros A, Butt A, Loyau S, Jandrot-Perrus M, et al. Collagen can selectively trigger a platelet secretory phenotype via glycoprotein VI. *PLoS One*. 2014;9:e104712. https://doi.org/10.1371/journal.pone.0104712
[48] Alberio L, Safa O, Clemetson KJ, Esmon CT, Dale GL. Surface expression and functional characterization of alpha-granule factor V in human platelets: effects of ionophore A23187, thrombin, collagen, and convulxin. *Blood*. 2000;95:1694–702.
[49] Rivera J, Lozano ML, Navarro-Núñez L, Vicente V. Platelet receptors and signaling in the dynamics of thrombus formation. *Haematologica*. 2009;94:700–11.
[50] Merten M, Thiagarajan P. P-selectin expression on platelets determines size and stability of platelet aggregates. *Circulation*. 2000;102:1931–6.
[51] Pelzl L, Singh A, Funk J, Witzemann A, Marini I, Zlamal J, et al. Antibody-mediated procoagulant platelet formation in COVID-19 is AKT dependent. *J Thromb Haemost*. 2022;20:387–98.
[52] Schaubaecher JB, Smiljanov B, Haring F, Steiger K, Wu Z, Ugurluoglu A, et al. Procoagulant platelets promote immune evasion in triple-negative breast cancer. *Blood*. 2024;144:216–26.
[53] Kirkpatrick AC, Vincent AS, Dale GL, Prodan CI. Increased platelet procoagulant potential predicts recurrent stroke and TIA after lacunar infarction. *J Thromb Haemost*. 2020;18:660–8.
[54] Josefsson EC, Ramström S, Thaler J, Lordkipanidzé M, COAGAPO study group. Consensus report on markers to distinguish procoagulant platelets from apoptotic platelets: communication from the Scientific and Standardization Committee of the ISTH. *J Thromb Haemost*. 2023;21:2291–9.
[55] Montague SJ, Andrews RK, Gardiner EE. Mechanisms of receptor shedding in platelets. *Blood*. 2018;132:2535–45.
[56] Roweth HG, Malloy MW, Goreczny GJ, Becker IC, Guo Q, Mittendorf EA, et al. Pro-inflammatory megakaryocyte gene expression in murine models of breast cancer. *Sci Adv*. 2022;8:eabo5224. https://doi.org/10.1126/sciadv.abo5224
[57] Jayachandran M, Miller VM, Brunn GJ, Owen WG. Platelet response as a sentinel marker of toll-like receptor 4 activation in mice. *Thromb Res*. 2010;126:414–7.
[58] Morodomi Y, Kanaji S, Sullivan BM, Zarpellon A, Orje JN, Won E, et al. Inflammatory platelet production stimulated by tyrosyl-tRNA synthetase mimicking viral infection. *Proc Natl Acad Sci U S A*. 2022;119:e2212659119. https://doi.org/10.1073/pnas.2212659119
[59] Zhang G, Han J, Welch EJ, Ye RD, Voyno-Yasenetskaya TA, Malik AB, et al. Lipopolysaccharide stimulates platelet secretion and potentiates platelet aggregation via TLR4/MyD88 and the cGMP-dependent protein kinase pathway. *J Immunol*. 2009;182:7997–8004.
[60] Lopes Pires ME, Clarke SR, Marcondes S, Gibbins JM. Lipopolysaccharide potentiates platelet responses via toll-like receptor 4-stimulated Akt-Erk-PLA2 signalling. *PLoS One*. 2017;12:e0186981. https://doi.org/10.1371/journal.pone.0186981
[61] Min BK, Suk K, Lee WH. Stimulation of CD107 affects LPS-induced cytokine secretion and cellular adhesion through the ERK signaling pathway in the human macrophage-like cell line, THP-1. *Cell Immunol*. 2013;281:122–8.
[62] Han Y, Liu D, Li L. PD-1/PD-L1 pathway: current researches in cancer. *Am J Cancer Res*. 2020;10:727–42.
[63] Hinterleitner C, Strähle J, Malenke E, Hinterleitner M, Henning M, Seehawer M, et al. Platelet PD-L1 reflects collective intratumoral PD-L1 expression and predicts immunotherapy response in non-small cell lung cancer. *Nat Commun*. 2021;12:7005. https://doi.org/10.1038/s41467-021-27303-7
[64] Zaslavsky AB, Adams MP, Cao X, Maj T, Choi JE, Stangl-Kremser J, et al. Platelet PD-L1 suppresses anti-cancer immune cell activity in PD-L1 negative tumors. *Sci Rep*. 2020;10:19296. https://doi.org/10.1038/s41598-020-76351-4
[65] Guo Q, Malloy MW, Roweth HG, McAllister SS, Italiano JE, Battinelli EM. Platelets upregulate tumor cell programmed death ligand 1 in an epidermal growth factor receptor-dependent manner in vitro. *Blood Adv*. 2022;6:5668–75.
[66] Guy A, Helzy K, Mansier O, Bordet JC, Rivière E, Fiore M, et al. Platelet function studies in myeloproliferative neoplasms patients with *Calreticulin* or *JAK2*^{V617F} mutation. *Res Pract Thromb Haemost*. 2023;7:100060. https://doi.org/10.1016/j.rpth.2023.100060
[67] Hobbs CM, Manning H, Bennett C, Vasquez L, Severin S, Brain L, et al. JAK2V617F leads to intrinsic changes in platelet formation and reactivity in a knock-in mouse model of essential thrombocythemia. *Blood*. 2013;122:3787–97.
[68] Arellano-Rodrigo E, Alvarez-Larrán A, Reverter JC, Villamor N, Colomer D, Cervantes F. Increased platelet and leukocyte activation as contributing mechanisms for thrombosis in essential thrombocythemia and correlation with the JAK2 mutational status. *Haematologica*. 2006;91:169–75.
[69] Marín Oyarzún CP, Glembotsky AC, Goette NP, Lev PR, De Luca G, Baroni Pietto MC, et al. Platelet toll-like receptors mediate thromboinflammatory responses in patients with essential thrombocythemia. *Front Immunol*. 2020;11:705. https://doi.org/10.3389/fimmu.2020.00705
[70] Li B, Lu Z, Yang Z, Zhang X, Wang M, Chu T, et al. Monitoring circulating platelet activity to predict cancer-associated thrombosis. *Cell Rep Methods*. 2023;3:100513. https://doi.org/10.1016/j.crmeth.2023.100513
[71] Falanga A, Marchetti M. Cancer-associated thrombosis: enhanced awareness and pathophysiologic complexity. *J Thromb Haemost*. 2023;21:1397–408.
[72] Tsantes AG, Petrou E, Tsante KA, Sokou R, Frantzeskaki F, Domouchtsidou A, et al. Cancer-associated thrombosis: pathophysiology, laboratory assessment, and current guidelines. *Cancers (Basel)*. 2024;16:2082. https://doi.org/10.3390/cancers16112082
[73] Naganuma Y, Satoh K, Yi Q, Asazuma N, Yatomi Y, Ozaki Y. Cleavage of platelet endothelial cell adhesion molecule-1 (PECAM-1) in platelets exposed to high shear stress. *J Thromb Haemost*. 2004;2:1998–2008.
[74] Fornasa G, Groyer E, Clement M, Dimitrov J, Compain C, Gaston AT, et al. TCR stimulation drives cleavage and shedding of the ITIM receptor CD31. *J Immunol*. 2010;184:5485–92.
[75] Jayachandran M, Hashimoto K, Brunn GJ, Owen WG, Miller VM. A single in vivo exposure to low-dose LPS decreases platelet lifespan through TLR4 in mice. *FASEB J*. 2007;21:A183.

SUPPLEMENTARY MATERIAL

The online version contains supplementary material available at https://doi.org/10.1016/j.rpth.2026.103371.